Autonomous Mars-Gravity Enabling Quadrotor

Kedarisetty Siddhardha [*]

[*] K. Siddhardha is with Department Aerospace Engineering, IIT Madras,
Chennai, India (e-mail: siddhardhak2010@gmail.com).

Abstract: Study of various physical phenomena in reduced gravity environments is of importance to several branches of science. This paper describes the trajectory design and automation control strategy for a quadrotor to maintain an acceleration such that a payload on-board experiences Mars-gravity for a short time period. A 1-D vertical trajectory with time varying acceleration is proposed for this purpose. A detailed kinematic analysis is presented to arrive at an acceleration schedule for the quadrotor to follow this trajectory. The analysis will also enable a designer to choose an appropriate motor-propeller combination for a quadrotor to follow this trajectory, given the constraints on peak altitude of the executed trajectory and duration for which reduced gravity needs to be maintained. The efficacy of the proposed approach and automation strategy is demonstrated using a detailed 6-DoF model simulation. Since the proposed trajectory is highly unsteady, the widely used steady state thrust model for quadrotors will not suffice. Therefore, a better thrust model is developed using blade element theory where the model parameters are estimated using experiments conducted in a wind tunnel. Our kinematic analysis shows that an appropriately designed quadrotor is capable of replicating Mars gravity environment for duration of 4 seconds while executing a vertical trajectory with peak altitude less than 45 m, which is validated through simulation and a preliminary flight test.

Keywords: Reduced gravity, quadrotor, autonomous control, system modelling.

1. INTRODUCTION

The study of fluid physics, flame and combustion characteristics, material science, and biotechnology under reduced-gravity (micro, Moon, and Mars) conditions is a major area of research (Ries-Kautt (1997); Alam (2016); Pletser (2012)). In order to simulate reduced gravity environments on Earth, researchers use drop towers, manned fixed wing aircraft, and rockets (Belser (2016); Pletser (2008)). Despite the high g-quality (lower the residual acceleration, higher the g-quality) and their capability to carry heavy payloads, these methods that simulate reduced-gravity environment are costly, and the procedures are involved limiting the frequency at which they can conducted (Afman (2016)).

Meanwhile, the advances in Unmanned Aerial Vehicle (UAV) technology, enabled researchers to conduct reduced gravity experiments at low cost and more frequently in spite of the reduced g-quality and lower payload capacity. In Higashino (2010), the authors proposed the use of a fixed wing UAV to create reduced gravity environment. The simulation results show that an environment less than $0.15g$ can be achieved for 2 to 3 seconds. Although the experimental results presented were not as satisfactory as the simulation results, the feasibility of using UAVs to produce reduced gravity was proved. In Hofmeister (2011), authors experimentally created micro-gravity using a fixed wing UAV for about 10 seconds. However, to achieve such duration of micro-gravity, the flight path length and the change in altitude required was 1 km and 400 meters respectively.

Moreover, owing to the wind conditions at such altitudes, the g-quality obtained was very poor (disturbance band of $0.4g$ magnitude). Unlike fixed wing UAVs, quadrotors can perform vertical maneouvres, thereby opening up the possibility of performing free-fall-like 1-D parabolic manoeuvres to create reduced gravity environments (Afman (2016)). A novel conceptual approach of using a variable pitch propeller quadrotor to achieve a micro-gravity environment is proposed in Afman (2016). Their simulation results show that it is possible to achieve a micro-gravity for about 3 seconds. A variable pitch propeller quadrotor (instead of conventional quadrotor) is required because both positive and negative thrust forces are necessary to maintain micro-gravity as well as to maintain attitude control. This is, however, not possible to achieve by a conventional quadrotor. A conventional quadrotor requires to switch of the propeller rotation to achieve free fall, thus leaving the quadrotor uncontrollable to disturbances. Therefore, a conventional quadrotor cannot be used for simulating micro-gravity environments. However, it is possible to produce a reduced-non-zero-gravity environments with a conventional quadrotor.

The major focus of this work is to design an autonomous conventional quadrotor towards simulating Mars gravity environment on Earth. A 1-D parabolic (in time) manoeuvre is proposed to achieve the required gravity levels. The kinematics of this flight trajectory are derived with the consideration of flying constraints (maximum height, reduced gravity duration and payload). The kinematic analysis also provides a base for the choice of the motor-propeller combination for this mission. An automation

control strategy is proposed to enable the quadrotor to execute the desired trajectory autonomously. As the quadrotor has to perform ascent and descent flights to complete the proposed 1-D parabolic manoeuvre, a blade element theory based axial flight model is derived to calculate the thrust and counter torque of a propeller in axial flights. To validate the derived model in axial flight conditions and to estimate model parameters, wind-tunnel experiments are conducted. Finally, simulation and preliminary flight test results are presented to demonstrate the capability of conventional quadrotors to simulate reduced gravity environments.

2. TRAJECTORY DESIGN

One way to create reduced gravity using a fixed wing aircraft is to perform a 2-D parabolic manoeuvre. Fixed wing aircraft require forward speed to be airborne, and therefore, to simulate a reduced gravity environment, they need to have a flight trajectory that spreads along both forward and vertical translational axes. However, owing to its capability to translate only along the vertical axis, a quadrotor can perform a 1-D parabolic (in time) manoeuvre to achieve reduced gravity.

2.1 The Trajectory

The proposed trajectory a quadrotor need to follow to create Mars-gravity is shown in Fig. 1, and can be divided into five phases. In the first (take-off) phase, quadrotor takes off from ground and hovers at a certain altitude. In the second (climb) phase, it accelerates to reach a certain desired velocity. Once this velocity is achieved, the rotor angular speeds are varied such that the desired constant acceleration is maintained (third phase - reduced gravity phase). After completing the parabolic path, the quadrotor accelerates to break the fall in phase four (decent phase), and performs a controlled landing in phase five (landing phase). These five phases are indicated in Fig. 1. The circled number in the figure marks the beginning of the corresponding phase.
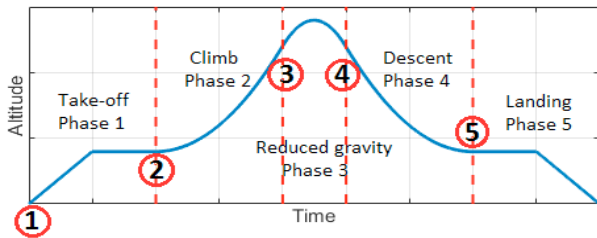
Fig. 1. Phases of 1-D parabolic manoeuvre

2.2 Flying Constraints

There are three constraints that has to be considered while designing a quadrotor to conduct reduced gravity experiments.

- Peak altitude (h_{peak}): It is the maximum altitude a quadrotor achieves while executing the proposed trajectory. The peak altitude contraint usually arise from governmental regulations on UAV flying. For

example, as per the Indian government regulations, the maximum altitude at which a micro UAV (weight less than 2 kg) can fly in an educational/ research institution without local authority permission is 200 ft (60 m approximately) (Air Transport Circular (2016)).
- Reduced gravity time (t_{rg}): It is the amount of time the quadrotor spends in a reduced gravity state.
- Payload mass (m_p): It is the mass of the on-board equipment required to conduct experiments while in reduced gravity state.

2.3 Kinematics

A detailed kinematic analysis is performed to compute the acceleration schedule required for a quadrotor to follow the proposed 1-D trajectory. First, the kinematic equations for phase-3 – the reduced gravity phase – is derived, as the required accelerations in the other phases, especially the desired acceleration in climb phase, will depend upon this.

Phase-3 The acceleration experienced by a payload on-board is

$$a_{exp} = a_E - a_b \tag{1}$$

where, a_E is gravitational acceleration of Earth, and a_b is the acceleration of the body (quadrotor). We have

$$a_b = a_f + a_E \tag{2}$$

where, a_f is the body acceleration due to thrust and drag forces acting on it.

For the purpose of this paper, the required experienced acceleration a_M – the acceleration due to gravity on Mars. From the equations (1) and (2), the desired acceleration due to thrust of the rotors (we neglect drag in this analysis) is

$$a_f = -a_M \tag{3}$$

From the kinematic equations for one dimensional motion, we obtain

$$h_{peak} = h_3 - \frac{1}{8}a_{rg}t_{rg}^2, \quad v_3 = -v_5 = -\frac{a_{rg}t_{rg}}{2} \tag{4}$$

where, h_i and v_i are respectively the altitude and velocity at the beginning of phase-i, t_{rg} is the duration of phase-3, and $a_{rg} = a_f + a_E = -a_M + a_E$ is the body acceleration in phase-3.

Phase-2 The kinematic equations for phase-2 gives us

$$h_3 = h_2 + \frac{a_{rg}^2 t_{rg}^2}{8a_{23}}, \quad t_{23} = -\frac{a_{rg}t_{rg}}{2a_{23}} \tag{5}$$

where, t_{23} is the duration of phase-2, and a_{23} is body acceleration in phase-2. Note that in deriving the above relations, we used v_3 from equation (4).

From equations (4) and (5), we can obtain the acceleration requirement and its duration in phase 2, given the constraints on h_{peak} and t_{rg} as

$$a_{23} = \frac{a_{rg}^2 t_{rg}^2}{8(h_{peak} - h_2) + a_{rg}t_{rg}^2}, \quad t_{23} = -\frac{a_{rg}t_{rg}}{2a_{23}} \tag{6}$$

Assuming a hover altitude of 5 m (h_2) and using the above derived relations, we have computed the peak altitude

and the time duration of phase 2 (t_{23}) as a function of acceleration requirement in phase 2 (a_{23}) for various values of reduced gravity duration. These are plotted in Fig. 2. These charts will help a designer to estimate the maximum acceleration requirement, given the h_{peak} and t_{rg} constraints, to make an appropriate motor-propeller selection as described in the next section.

(a) h_{peak} vs a_{23}

(b) t_{23} vs a_{23}
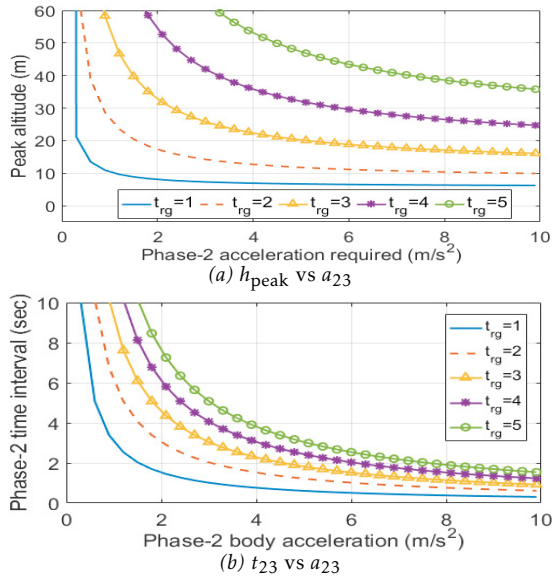
Fig. 2. Design charts obtained from kinematic analysis

3. MOTOR-PROPELLER SELECTION

Unlike the general quadrotor design for which the major design criteria are agility, range and endurance, the design criterion for a quadrotor to create reduced gravity is the ability to produce required acceleration in the ascent and descent phases. Thus the quadrotor should be designed such that maximum thrust produced by the motor-propeller combination meets this requirement. Fig. 2a provides the acceleration requirement (a_{23}) in ascent and descent phases given the h_{peak} and t_{rg} constraints. Given this, the acceleration that the motor-propeller combination should produce is obtained from equation (2) as

$$a_f = a_{23} - a_E \qquad (7)$$

Thus, the minimum thrust constraint can be written as

$$T \geq k_s m_q a_f \qquad (8)$$

where, k_s is the safety factor taken as 1.5 in practice. Here, the quadrotor mass m_q is

$$m_q = 4m_a + m_k + m_p \qquad (9)$$

where, m_p is the payload mass, m_k is the known mass, that is, the mass of the battery, frame, electronics, etc., and m_a is the mass of motor-propeller module.

Thus, any motor-propeller combination that satisfies the following constraint can be chosen of this mission

$$T \geq k_s(4m_a + m_k + m_p)a_f \qquad (10)$$

Note that this is a 'design relation' wherein the quantities on both the right hand side (T) and the left hand side (m_a) depends on the choice of motor-propeller combination.

4. CONTROL AND AUTOMATION STRATEGY

From the kinematic analysis presented in Section 2, the acceleration schedule – acceleration value and duration for each phase – is known, which when followed will result in the on-board payload experiencing reduced gravity (Mars-gravity in our case) for the required duration. To implement this acceleration schedule on a quadrotor with the motor and propeller appropriately chosen as in the previous section, we propose the following control and automation strategy. We propose to use a low-level attitude controller and higher level automation (altitude-acceleration controller for various flight phases) as described below.

4.1 Attitude Control
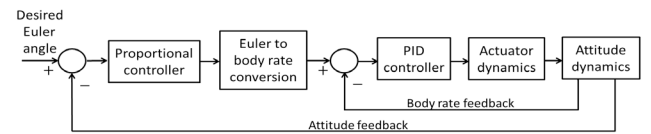
Fig. 3. Attitude controller structure

A 2-loop feedback control structure is chosen for attitude controller as shown in Fig. 3. An outer loop with attitude feedback, and an inner loop with body rate feedback makes this control structure robust to disturbances such as model uncertainties, measurement noise, and environmental disturbances.

4.2 Automation
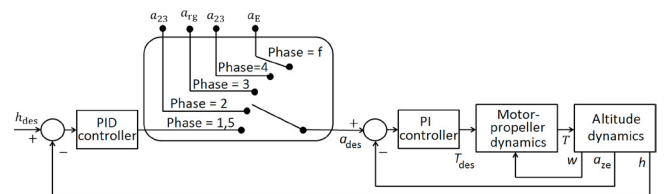
Fig. 4. Automation strategy

To enable a quadrotor to autonomously fly the five phases of the proposed reduced gravity manoeuvre, we suggest a state machine like automation as shown in Fig. 4. Depending upon the current phase, the desired acceleration is provided to a PI controller that uses an acceleration feedback to generate appropriate command to be given to the motor-propeller module. For take-off and landing phases (1 and 5), the desired acceleration is generated by an outer PID loop executing an altitude hold (see Fig. 4). In the climb, reduced gravity and decent phases (2, 3, and 4) required acceleration obtained from the kinematic analysis is used as desired acceleration input to the PI controller.

In the case of communication loss or loss of stability, the phase state will be set as 'fault' (Phase f), and the desired acceleration is given as the acceleration due to gravity of Earth. This results in shutting down of all the motors and a resultant free-fall.

5. SYSTEM MODELLING

The quadrotor governing equations of motion, and the propeller thrust and counter torque model used in simulations to test the proposed automation strategy are described in this section.

5.1 Governing Equations

We use the standard rigid body equations, specialized for quadrotors, given as

$$\frac{d(mV_b)}{dt} + \Omega_b \times (mV_b) = F_p + F_g$$
$$\frac{d(I\Omega_b)}{dt} + \Omega_b \times (I\Omega_b) = \tau_{cg} + \tau_p + \tau_{gp} \quad (11)$$

where, V_b and Ω_b are the translation and angular velocities in directions of body reference frame axes, m is the mass of quadrotor, and I is the rotational inertia matrix of the quadrotor. The description of the forces and torques on the right hand side of equation (11) are as follows: F_b - force due to propeller, F_b - force due to gravity, τ_{cg} - torque due to center of gravity shift from geometric center, τ_p - torque due to propellers, and τ_{gp} - torque due to propeller gyroscopic effects.

The widely used and popular thrust model for quadrotor assumes that the thrust produced is directly proportional to the square of RPM (Bouabdallah (2004)). This is true in hover and when the quadrotor is translating steady at very low speeds which usually is the case. However, our proposed trajectory involves varying accelerations and speeds as seen in Section 2, such a thrust model will not suffice. Therefore, we propose a new thrust model, that is more appropriate when axial speeds are non-zero, using blade element theory.

5.2 Thrust model

To develop a model that predicts the thrust and counter torque produced by a propeller in axial flights, we use the theory of blade element analysis (Leishman (2006)). Consider a propeller with solidity ratio σ, effective lift coefficient slope $c_{l\alpha}$, blade pitch θ, non-dimensional inflow velocity λ_i, and non-dimensional axial velocity λ_a due to ascent or decent. Then from the blade element analysis, the elemental thrust coefficient can be written as (Leishman (2006))

$$dC_T = \frac{1}{2}c_{l\alpha}\sigma r^2\left[\theta - \left(\frac{\lambda_i + \lambda_a}{r}\right)\right] \quad (12)$$

where r is the non-dimensional radius of the propeller ($r \in [0,1]$).

The solidity ratio (σ) is constant for rectangular blades. However, for usual propellers σ varies along the length of the blade as the chord length is not constant. Similarly, the twist of the blade also varies along the blade length. For analysis, we assume second order polynomials to model the variation of σ and θ along the blade as

$$\sigma = \sum_{i=0}^{2}\sigma_i r^i; \quad \theta = \sum_{i=0}^{2}\theta_i r^i \quad (13)$$

Substituting in equation (12), we get

$$dC_T = \frac{1}{2}c_{l\alpha}\left(\sum_{i=0}^{2}\sigma_i r^i\right)\left[r^2\left(\sum_{i=0}^{2}\theta_i r^i\right) - r(\lambda_i + \lambda_a)\right]dr \quad (14)$$

By integrating along the blade length, the total thrust coefficient can be obtained as

$$C_T = \frac{1}{2}c_{l\alpha}\left[k_1 + k_2\left(\lambda_i + \lambda_a\right)\right] \quad (15)$$

where, the constants k_1 and k_2 are functions of solidity ratio and pitch function coefficients $\sigma_i, \theta_i, i = 0, 1, 2$. Thus, the total thrust produced by a propeller of radius R can be obtained by using the relation between thrust and non-dimensional thrust coefficient $T = C_T\rho\pi R^2(\omega R)^2$ as

$$T = \left[\frac{1}{2}c_{l\alpha}\left(k_1 + \frac{k_2 v_i}{\omega R}\right)\pi R^4\right]\omega^2 + \left[\frac{1}{2}c_{l\alpha}k_2\pi R^3\right]\omega V_a \quad (16)$$

The relation between the inflow velocity and angular speed of the propeller is linear ($v_i = k_v\omega$). This can be verified experimentally as shown in Fig. 6(b). Therefore, the thrust produced by the propeller in axial flight can be written as

$$T = b\omega^2 + b_a\omega V_a \quad (17)$$

where, $b = \frac{1}{2}c_{l\alpha}\left(k_1 + \frac{k_2 k_v}{R}\right)\pi R^4$ and $b_a = \frac{1}{2}c_{l\alpha}k_2\pi R^3$ are hover thrust and axial thrust coefficients respectively.

(a) Wind tunnel

(b) Motor-propeller setup
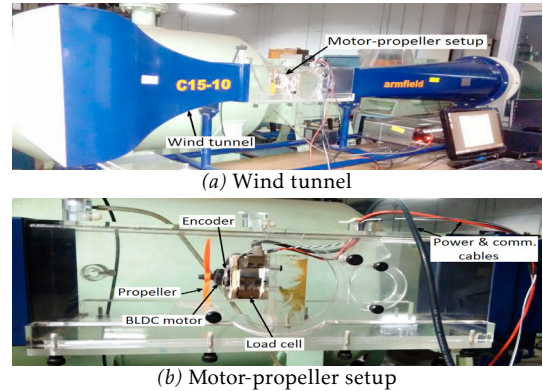
Fig. 5. Wind-tunnel experimental setup

In order to experimentally validate the developed theoretical expressions, and to find the thrust coefficients, a sub-sonic wind tunnel is used to simulate the descent flight conditions for a propeller as shown in Fig. 5(a). The wind tunnel is capable of producing inflow velocity upto 12 m/s inside the chamber. The set-up inside the wind tunnel chamber as shown in Fig. 5(b) consists of motor-propeller combination, a six axis load cell to measure the thrust and counter torque, and an encoder to measure the angular speed of the propeller.

In order to examine the wall-effects on motor-propeller inside the wind tunnel, the values of T, ω and v_i are measured without any opposing inflow from wind tunnel (hover condition). The variation of these readings from the measurements obtained outside the wind tunnel are negligible. Thereby, in further wind-tunnel experiments, the wall-effect on motor-propeller module is considered to be negligible. The steady state measurements of T vs ω, and v_i vs ω under hover condition are provided in

(a) T vs ω at hover

(b) v_i vs ω at hover
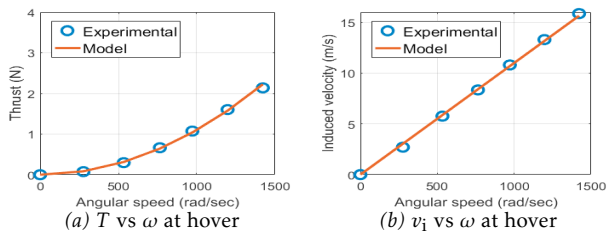
Fig. 6. Steady state thrust and inflow response of propeller at hover

Fig. 6(a) and 6(b) respectively. From the Fig. 6(b), we can observe that the relation between inflow velocity and motor angular speed is linear ($v_i = k_v \omega$).

(a) T vs ω at $v_a = -6\,\mathrm{m/s}$

(b) T vs ω at $v_a = -7.3\,\mathrm{m/s}$

(c) T vs ω at $v_a = -8.5\,\mathrm{m/s}$

(d) T vs ω at $v_a = -9.8\,\mathrm{m/s}$
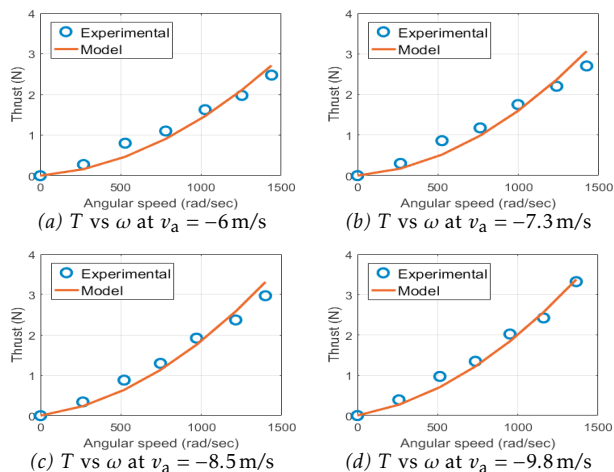
Fig. 7. Steady state thrust measurements under descent condition

To obtain thrust model coefficients (b and b_a), the measurements of T vs ω for various opposing airflow velocities are recorded as shown in Fig. 7. The combination of vehicle governing equations, motor dynamics, and thrust and counter torque steady state models completes the mathematical modelling of quadrotor in axial flights. This complex non-linear model is used for simulation purposes in the sections that follow.

6. RESULTS

To demonstrate the efficacy of our proposed approach to generate reduced gravity using quadrotors, we perform a 6DoF simulation implementation of the suggested strategy. To validate the simulation results, preliminary (open-loop) experimental flight test results are also presented.

6.1 Simulation results

The altitude, axial velocity and acceleration, and propeller angular speed simulation results for autonomous reduced gravity manoeuvre are shown in Fig. 8. In these plots, the transition in flight phase is indicated using a vertical dash line.

Operation In the take-off phase, the quadrotor is commanded to hover at a height of 5 m. After achieving

steady state (triggering criteria for phase 2), desired body acceleration of a_{23} (3.01 m/s^2) is provided as command input. After achieving desired climb velocity (v_3 (12.1 m/s), the flight transitions to reduced gravity phase. In the reduced gravity phase the commanded body ac-
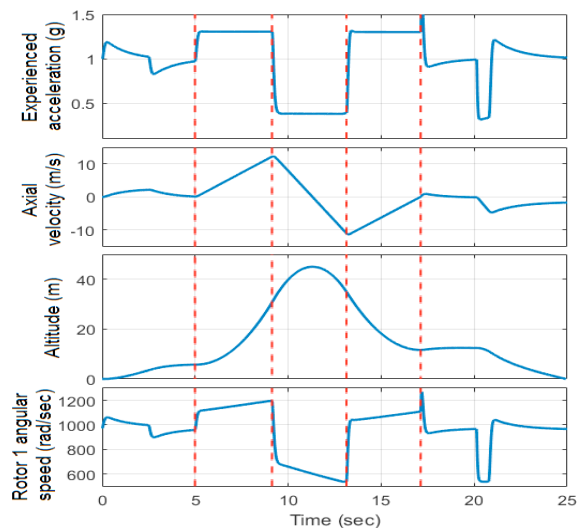
Fig. 8. Simulation plots

celeration is a_{rg} (−6.099 m/s^2), and the experienced acceleration on the quadrotor in this phase will mimic the Mars gravity. After t_{rg} (4 seconds) time period of reduced gravity phase (triggering criteria for phase 4), the descent phase is commenced by providing body acceleration command of a_{23} to break the fall. The descent phase is switched to landing phase once the velocity approaches near to zero.

Analysis In order to maintain a constant acceleration in phases 2,3 and 4, the angular speed of the rotor is varied such that a constant thrust is achieved. In climb phase (refer rotor angular speed plot in Fig. 8), as the axial airflow increases, the angular speed of the propeller is increased such that a constant acceleration is produced. This is because in ascent the thrust produced by the propeller decreases when compared to the thrust produced in hover condition at same angular speeds. Similarly, during reduced gravity phase, as the quadrotor velocity decreases, the angular speed of the rotor also decreases to maintain constant thrust. Thus, the proposed autonomous flight strategy helps to produce a constant Mars gravity environment.

6.2 Flight Test Results

Implementation In flight tests, a 3 phase open loop acceleration control is used to conduct preliminary reduced gravity experiments. The ascent, reduced gravity and descent are the three phases in the flight envelope. Based on the desired acceleration in each phase, BLDC motors are commanded appropriately (to produce desired thrust under hover conditions) for the calculated time interval using kinematics in Section 2. In the ascent and reduced gravity phases, the thrust command is autonomous, that is, for given time interval of each phase, desired actuation signals are provided to BLDC motors by the au-

topilot code. Whereas, at the end of the reduced gravity phase, the quadrotor thrust control is switched to remote control. An experienced human pilot ensures the safe landing of the quadrotor by providing appropriate thrust commands.
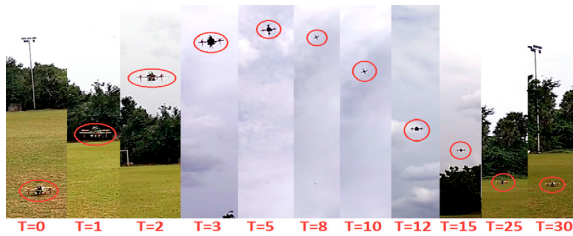
Fig. 9. Flight test
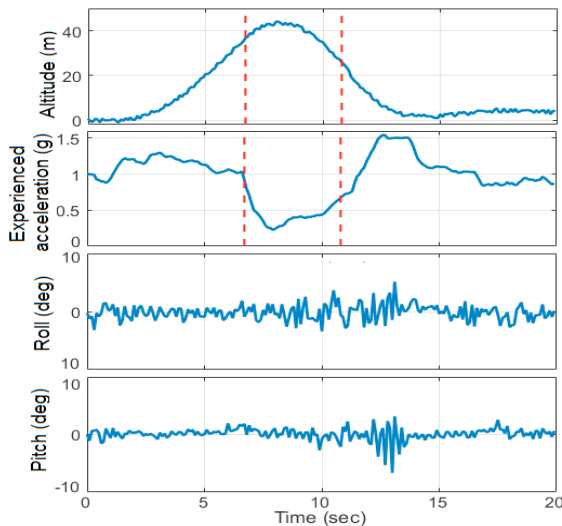
Fig. 10. Altitude, acceleration, and attitude plots

Results and analysis   The flight test snapshot collage of the quadrotor performing a 1-D parabolic like manoeuvre is shown in Fig. 9. The corresponding altitude, acceleration, and attitude plots are shown in Fig. 10. We can observe from Fig. 10(b) that a reduced gravity phase replicating the Mars gravity lasted approximately 4 seconds, and the peak altitude is within the prescribed limit. The designed attitude controller maintained the attitude of the vehicle within the range of ±3 degrees with an exception of a small disturbance oscillation due to sudden increase in the vehicles thrust.

From the altitude and acceleration plots we can observe that the altitude does not decrease instantaneously with decrease in acceleration during the transition from acceleration to reduced gravity phase. This is due to the existing momentum of the body at the end of the acceleration phase, which enables the quadrotor to complete a 1-D parabolic like path.

Since an open loop acceleration control strategy is chosen instead of closed loop control, the desired acceleration could not be maintained. From the analysis plot Fig. 12(b), in the ascent phase, the acceleration of the body decreases as the thrust produced by the propellers are decreased due to the upward axial flow. Similarly, in reduced gravity phase, we can observe increase in the

acceleration towards the phase end, which is due to the thrust increase of the propeller caused by the downward axial velocity.

These deviations in the acceleration can be easily controlled by implementing the developed autonomous strategy. Therefore, the preliminary flight test results indicate that the conventional quadrotors are feasible and capable to replicate reduced gravity environments with the exception of micro-gravity.

7. CONCLUSIONS

In this paper, the design, modelling and automation of conventional quadrotor capable of replicating Mars gravity environment is proposed. An approximate thrust model is derived using blade element theory and validated through series of wind tunnel experiments. The simulations confirmed the feasibility of using the conventional quadrotor and the developed automation strategy to create Mars gravity for duration of 4 to 5 seconds. The practicality of this concept is also verified through preliminary flight test results.

REFERENCES

Ries-Kautt, M., et al.   Crystallogenesis studies in microgravity with the Advanced Protein Crystallization Facility on SpaceHab-01. *Journal of crystal growth*, 181: 79–96, 1997.

Alam, F. E., Frederick, L. D., & Tanvir, I. F. Effectiveness of xenon as a fire suppressant under microgravity combustion environment. *Journal of Combustion Science and Technology*, 188:145–165, 2016.

Pletser, V., et al.   The first joint European partial-g parabolic flight campaign at Moon and Mars gravity levels for science and exploration. *Journal of Microgravity Science and Technology*, 24:1-13, 2012.

Belser, V., et al. Aerodynamic and engineering design of a 1.5 s high quality microgravity drop tower facility. *Acta Astronautica*, 129, pp. 335-344, 2016.

Pletser, V., Anne, P., & Olivier, M. International heat and mass transfer experiments on the 48th ESA parabolic flight campaign of March 2008. *Journal of Microgravity Science and Technology*, 20, pp. 177-182, 2008.

Higashino, S., & Shotaro, K.   Automatic Microgravity Flight System and Flight Testing Using a Small Unmanned Aerial Vehicle. *Journal of Japan Society Microgravity Application*, 27, pp. 3-10, 2010.

Hofmeister, P. G., & Jrgen, B. Parabolic flights@ home. *Journal of Microgravity Science and Technology*, 23, pp. 191-197, 2011.

Afman, J. P., et al. On the Design and Optimization of an Autonomous Microgravity Enabling Aerial Robot. *arXiv preprint*, arXiv:1611.07650, 2016.

Air Transport Circular. Office of the Director General of Civil Aviation, Government of India, 2016.

Nelson, R. C. *Flight stability and automatic control: Vol. 2.* New York: WCB/McGraw Hill, 1998.

Bouabdallah, S., Noth, A., & Siegwart, R. PID vs LQ control techniques applied to an indoor micro quadrotor. In *Proc. of International Conference on Intelligent Robots and Systems*, Sendai, Japan, pp. 2451-2456, 2004.

Leishman, G. J.   *Principles of helicopter aerodynamics*, Cambridge university press, 2006.